Evidence that pair breaking at the grain boundaries of $Bi_2Sr_2Ca_2Cu_3O_x$ tapes determines the critical current density above 10 K in high magnetic fields

1994 J. Phys.: Condens. Matter 6 10053

(http://iopscience.iop.org/0953-8984/6/46/022)

J. Phys.: Condens. Matter 6 (1994) 10053–10066. Printed in the UK

Evidence that pair breaking at the grain boundaries of $Bi_2Sr_2Ca_2Cu_3O_x$ tapes determines the critical current density above 10 K in high magnetic fields

L Le Lay†§, C M Friend†, T Maruyama‡, K Osamura‡ and D P Hampshire†

† Superconductivity Group, Department of Physics, University of Durham, South Road, Durham DH1 3LE, UK

‡ Department of Metallurgy, Kyoto University, Sakyo-ku, Kyoto 606, Japan

Received 17 May 1994, in final form 18 August 1994

Abstract. The critical current density of an aligned Ag doped $Bi_2Sr_2Ca_2Cu_3O_x$ tape has been measured from 10 K up to T_c (105 K) in magnetic fields up to 15 T. Measurements of the critical current density ($J_c(B, T)$) have been completed for three different configurations of magnetic field, transport current, and superconducting tape: (i) $J \perp c$ axis, $J \perp B$, and $B \perp c$ axis; (ii) $J \perp c$ axis, $J \perp B$, and $B \parallel c$ axis; (iii) $J \perp c$ axis, $J \parallel B$, and $B \perp c$ axis. In all three configurations at high magnetic fields up to 15 T, we find the critical current density can be described by $J_c(B, T) = \alpha(\phi, T) \exp[-\mu_0 H/\beta(\phi, T)]$ where $\beta(\phi, T)$ is of a separable variable form $\beta(\phi, T) = \beta^{\#}(T)/f(\phi)$ where $\beta^{\#}(T)$ is a function of temperature alone and $f(\phi)$ is a constant dependent only on the orientation of B, J, and the c axis.

A similar but not identical exponential magnetic field dependence has been found in $Bi_2Sr_2Ca_2Cu_3O_x$, $Bi_2Sr_2CaCu_2O_x$, and $YBa_2Cu_3O_y$ thin films. We discuss the evidence that the exponential magnetic field dependence suggests that a pair breaking mechanism operates at barriers in these materials. We conclude that the grain boundaries determine $J_c(B, T)$ in the $Bi_2Sr_2Ca_2Cu_3O_x$ textured tape.

1. Introduction

There is an enormous effort in the superconductivity community directed at understanding the magnetic field and temperature dependence of the transport critical current ($J_c(B, T)$) of high-temperature superconductors [1–8]. The interest lies in both understanding the fundamental mechanisms limiting $J_c(B, T)$ and increasing $J_c(B, T)$ for high-magnetic-field and high-power applications.

In the period after the discovery of high-temperature superconductors, while the materials science of these new materials was poorly understood, there was no clear understanding of the effect of fabrication and microstructure on $J_c(B, T)$. More recently, a clearer picture of how these factors are correlated has been developed in bulk aligned tapes optimized for high-current-density applications [3, 9]. In this work we extend the field and temperature range over which $J_c(B, T)$ has been measured in textured $Bi_2Sr_2Ca_2Cu_3O_x$ tapes.

The critical current density of a highly aligned Ag doped $Bi_2Sr_2Ca_2Cu_3O_x$ tape has been measured in detail from 10 K up to T_c in magnetic fields up to 15 T. Measurements of J_c have been completed for three different configurations of magnetic field, transport current,

§ Present address: BICC Pyrotenax Ltd, Hedgeley Road, Hebburn, Tyne and Wear NE31 1XR, UK.

0953-8984/94/4610053+14$19.50

and superconducting tape: (i) $J \perp c$ axis, $J \perp B$, and $B \perp c$ axis; (ii) $J \perp c$ axis, $J \perp B$, and $B \| c$ axis; and (iii) $J \perp c$ axis, $J \| B$, and $B \perp c$ axis. The magnitude of the critical current density is about 6×10^4 A cm^{-2} at 10 T and 4.2 K, which is typical of high-quality textured $Bi_2Sr_2Ca_2Cu_3O_x$ powder in tube tapes [4–8].

In the next section we outline the fabrication procedure for the tapes. In section 3 we describe the experimental procedure to measure variable-temperature voltage–current characteristics in high magnetic fields. In section 4 we present the raw critical current data. Section 5 presents a mathematical description and analysis of the data. In section 6, we compare the results we have obtained with those on $Bi_2Sr_2Ca_2Cu_3O_x$, $Bi_2Sr_2CaCu_2O_x$ and $YBa_2Cu_3O_y$ thin films. In section 7, we critically discuss some of the mechanisms suggested for determining $J_c(B, T)$. We discuss the evidence that a pair breaking mechanism operates at barriers in these materials and more specifically at the grain boundaries in the textured tape.

2. Sample preparation

In a separate study, a series of samples were introduced to investigate the influence of Ag additions on both the high-field properties of J_c at 4.2 K and the mechanical properties of the tapes [10]. It was found that J_c at 4.2 K and 10 T peaked at 6×10^4 A cm^{-2} with about 10 wt% Ag. We have chosen this optimized tape for the detailed investigation presented in this work.

High-purity powders of Bi_2O_3, PbO, $SrCO_3$, $CaCO_3$, and CuO were weighed and mixed in molar ratios of Bi:Pb:Sr:Ca:Cu of 1.6:0.4:1.6:2.0:2.8. The powders were calcined at 1073 K for 43.2 ks and ground for 10.8 ks. The calcination and grinding process was repeated a second time. After the second grinding 10 wt% Ag (Ag_2O powder) was added and mixed. The resultant powder was inserted into an Ag tube of 6 mm outer diameter and 1 mm thickness. Initially the wire was reduced by grove rolling. Then the wire was cold pressed with a uniaxial pressure of 900 MPa and heat treated at 1113 K for 540 ks. An additional cycle of uniaxial pressing at 900 MPa and heat treatment at 1113 K for 540 ks completed the thermomechanical heat treatment. The final sample was 80 μm thick, 2 mm wide, and 22 mm long. The cross-sectional area of the 10 wt% Ag doped $Bi_2Sr_2Ca_2Cu_3O_x$ core has a height:width aspect ratio of about 25 and an area of 6.2×10^{-4} cm^2.

The detailed microstructure of the tape is complex but similar to other tapes produced using this fabrication technique [9]. The superconducting core is strongly textured such that the plate like grains are aligned with their basal plane preferentially parallel to the broad face of the tape. A characterization of the tape using SEM, EPMA, and XRD has been completed and reported elsewhere [10].

3. Experimental details

The basic measurement consists of holding the applied magnetic field and the temperature constant while increasing the current passing through the superconductor and monitoring the voltage across two voltage taps attached to it. Initially no voltage is detected. Eventually there is a sharp increase in the voltage at the critical current. The critical current is recorded and the process is repeated at all required fields and temperatures.

We have recently commissioned a probe for making variable-temperature critical current measurements on both low-temperature and high-temperature superconductors in our

dedicated 17 T magnet system [11, 12]. The probe incorporates a heater, a high-precision Rh–Fe standard thermometer, and a field independent capacitance thermometer, which are all in intimate thermal contact with the superconductor. Initially the heater and the Rh–Fe thermometer are used to obtain the required temperature. Temperature control is then transferred to the field independent capacitance thermometer, which is in a closed cycle feedback loop with the heater and maintains the temperature while the voltage–current (V–I) characteristics are being measured or the magnetic field is being changed. After all the measurements at a given temperature have been completed, the magnetic field is reversed to −2 T and slowly reduced to zero before measurements are initiated at a new temperature. V–I characteristics can be obtained on superconducting thin films, wires, and tapes from 2 K up to T_c with a typical noise of 100 nV peak to peak. The instrumentation is computer controlled using IEEE-488 and RS232 protocols such that the raw V–I data are automatically digitized for ease of subsequent analysis.

The magnitude of $J_c(B, T)$ at 77 K in zero magnetic field is $\sim 8 \times 10^3$ A cm^{-2}, the same as found during the optimization work on these tapes [10]. We note the marked increase at 10 T from $\sim 7 \times 10^3$ A cm^{-2} at 10 K in this work to $\sim 6 \times 10^4$ A cm^{-2} at 4.2 K in the previous study [10]. In this work, we do not consider $J_c(B, T)$ data at temperatures below 10 K. Nevertheless, recently we have made measurements on other $Bi_2Sr_2Ca_2Cu_3O_x$ tapes and have found a similar marked increase in $J_c(B, T)$ below 10 K, which is consistent with the results in this paper.

For this $Bi_2Sr_2Ca_2Cu_3O_x$ tape the voltage taps were soldered 3 mm apart. We have taken an electric field criterion of 2 μV cm^{-1} to define the critical current. This criterion has been chosen to be as low as possible while maintaining good signal to noise. The magnetic field values quoted are accurate to one part in 10^5. The current through the superconductor is determined by measuring the voltage across a standard resistor and is accurate to better than 0.1%. We expect all values of critical current quoted in this paper to be accurate to better than 5%.

At the beginning of these measurements and after each data set for a given configuration had been completed, the critical current of the tape was measured in zero field in liquid nitrogen at 77 K. We found no change in the critical current of the sample and took this as evidence that no damage to the sample occurred during these measurements from sample mounting, Lorentz forces, or thermal cycling.

4. Experimental results

In figure 1 the critical current density defined at 2 μV cm^{-1} versus the magnetic field as a function of temperature is presented on a log–log plot. This format most clearly presents both the low-field and high-field data. The lines at each temperature serve as a guide to the eye. The transport current (J) is orthogonal to the c axis. The applied field is orthogonal to both J and the c axis and hence a macroscopic Lorentz force operates. In figures 2 and 3, the equivalent critical current data that have been obtained for the two other configurations considered in this work are presented. The following characteristics are common to all three figures: at low applied magnetic fields, while the self-field is larger than the applied field, J_c is independent of the applied field; at intermediate magnetic fields, J_c slowly decreases as the applied magnetic field increases; at high fields there is a marked decrease in J_c as the field increases.

The data in figures 1–3 have been replotted in figures 4–6 on log–linear plots. Although the detailed features of J_c at low magnetic fields are no longer clear in these figures, they

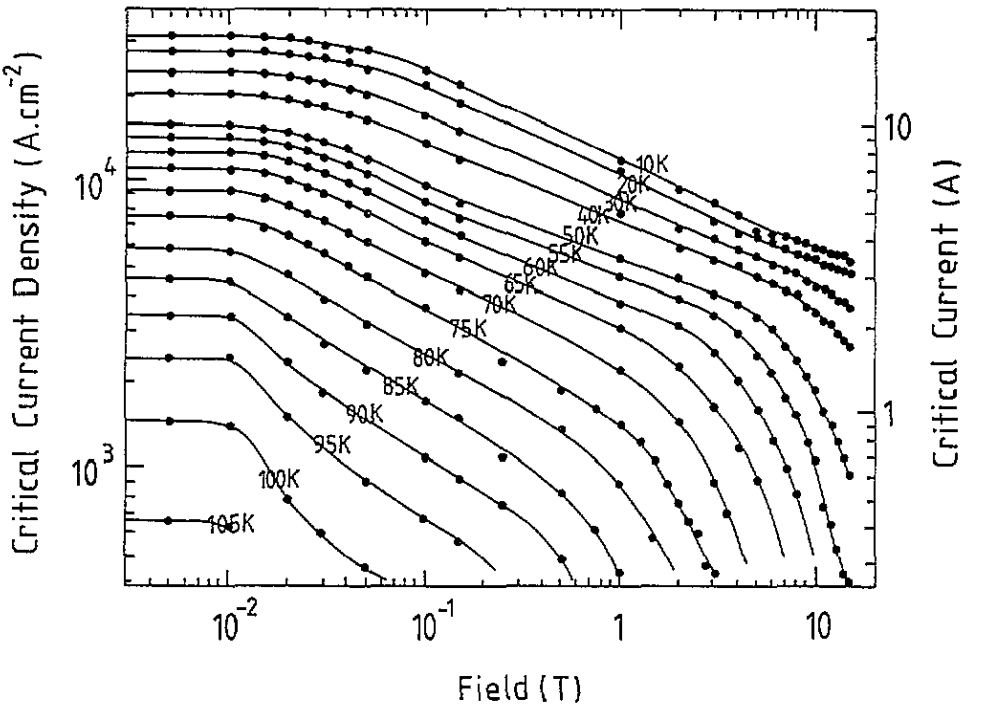

Figure 1. Log_{10} (critical current density) defined at 2 μV cm^{-1} versus $\log_{10}$ (magnetic field) as a function of temperature. J is orthogonal to the c axis. The applied field is orthogonal to both J and the c axis.

emphasize the high-field data, which are the focus of this paper. Figures 4–6 demonstrate that in high magnetic fields, at all temperatures for all three configurations the critical current exponentially decreases as the magnetic field increases. This exponential dependence holds whether the macroscopic Lorentz force operates (figures 4 and 5) or not (figure 6).

5. Analysis of data

5.1. Pair breaking

By considering the decay of the superconducting wavefunction through superconducting–normal–superconducting (S–N–S) junctions, De Gennes [13] found that the critical current has an exponential functional form given by

$$J_c(T) = J_0(1 - T/T_c)^2 \exp(-K_n d_n)$$

where J_0 is a constant, T_c is the critical temperature, d_n is the thickness of the normal layer, and K_n^{-1} is the characteristic decay length for the superconducting order parameter in the normal layer. This work has been extended by Hsiang and Finnemore [14] to include the magnetic field dependence of K_n using a phenomenological model such that when the normal metal is in the clean limit

$$J_c(B, T) = \alpha(T) \exp[-\mu_0 H/\beta(T)] \qquad (1)$$

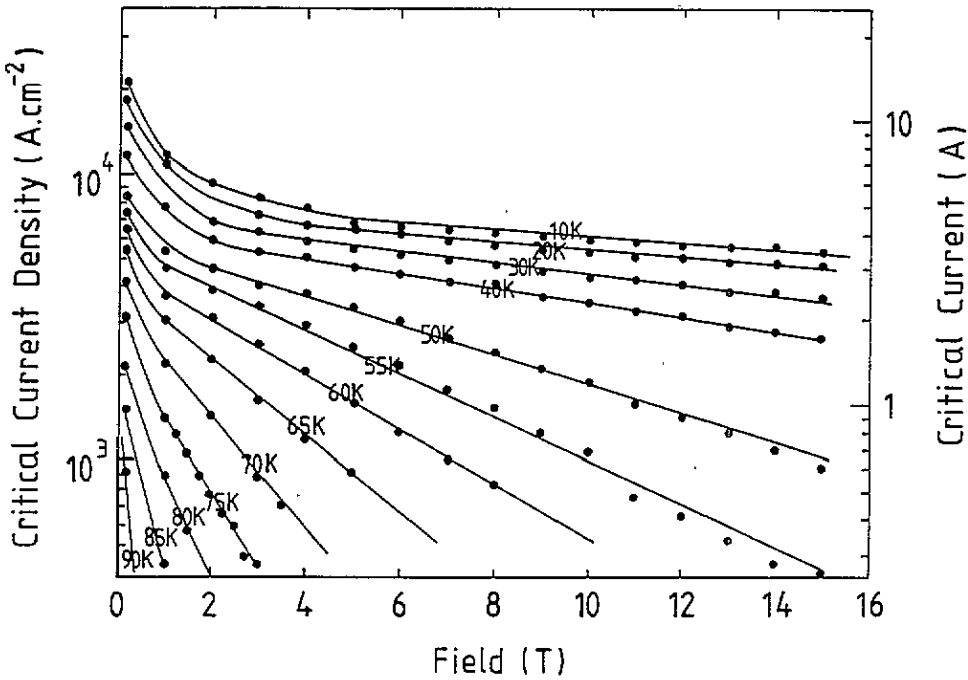

Figure 2. Log_{10} (critical current density) defined at 2 μV cm^{-1} versus log_{10} (magnetic field) as a function of temperature. J is orthogonal to the c axis. The applied field is parallel to J.

where the applied field is orthogonal to the direction of current flow, $\alpha(T)$ is a function of temperature alone and $\beta(T)$ is given by

$$\beta(T) = \hbar/\left(2\sqrt{3}eld\right) \tag{2}$$

where $\hbar = h/2\pi$ (h is Planck's constant), e is the electronic charge, l is the electron scattering length in the normal barrier, and d is the width of the barrier. The exponential dependence is a well known result from considering quantum mechanical tunnelling through a barrier.

Equation (1) describes the high-field $J_c(B, T)$ data in figures 4–6 for all three configurations. In figures 7 and 8, the temperature dependences of $\alpha(T)$ and $\beta(T)$ are presented.

In figure 7 the value of α has been determined by extrapolating the straight lines in figures 4–6 at high fields back to zero magnetic field. It should be noted that when the Lorentz force operates, the precipitous drop in $\alpha(T)$ for $B \perp c$, compared to $B \| c$, leads to a crossover in $\alpha(T)$ for these two configurations—the sensitivity of the temperature dependence of $\alpha(T)$ to the orientation of B and the c axis can be seen most obviously by noting that the intercepts of the straight lines are much closer in figure 4 than in figure 5 across the temperature range.

In figure 8, $\beta(T)$ is plotted as a function of temperature for the three configurations. In addition, for comparison, values of $\beta(T)$ derived from the work of Yamasaki *et al* [15] for a $Bi_2Sr_2Ca_2Cu_3O_x$ epitaxial thin film ($J \perp B$, $B \| c$ axis) are shown for comparison. The data in figure 8 are replotted in figure 9 on a log–linear plot. The solid lines drawn through

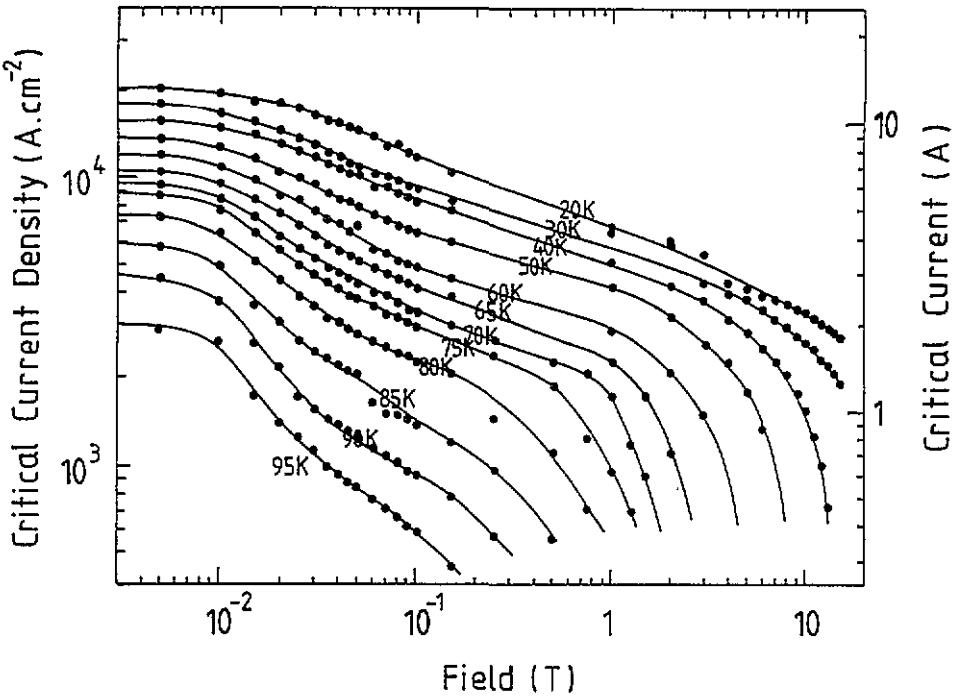

Figure 3. Log_{10} (critical current density) defined at 2 μV cm^{-1} versus $\log_{10}$ (magnetic field) as a function of temperature. J is orthogonal to the c axis. The applied field is parallel to the c axis.

our data in figure 9 have an identical temperature dependence but are displaced from each other. Hence our data are consistent with a single temperature dependence for $\beta(T)$:

$$\beta(J\|B,\ B\perp c)/2.6 = \beta(J\perp B,\ B\perp c)/1.65 = \beta(J\perp B,\ B\|c). \tag{3}$$

We can generalize (1) to include the orientation and temperature dependence of $\beta(T)$ in a separable variable form such that

$$J_c(B,T) = \alpha(\phi,T)\exp[-\mu_0 H/\beta(\phi,T)] \tag{4}$$

where $\beta(\phi,T)$ is of a separable variable form $\beta(\phi,T) = \beta^{\#}(T)/f(\phi)$ where $\beta^{\#}(T)$ is a function of temperature alone and $f(\phi)$ is a constant dependent only on the orientation of B, J, and the c axis.

5.2. *Flux pinning*

In low-temperature superconductors that have been optimized for high critical current density in high magnetic fields, it is well established that flux pinning mechanisms can determine J_c [16, 17]. The functional form of $J_c(B,T)$ is conventionally described using the Fietz–Webb [18] scaling law given by:

$$F_p = J_c B = \gamma B_{c2}^{n}(T) f(b) \tag{5}$$

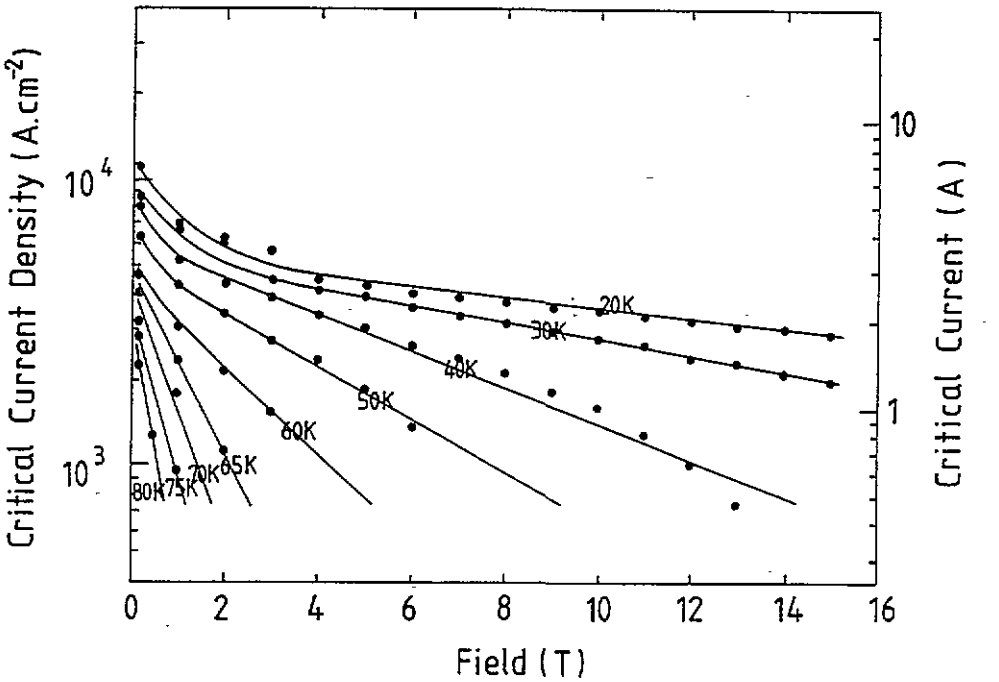

Figure 4. Log_{10} (critical current density) defined at 2 μV cm^{-1} as a function of field and temperature. J is orthogonal to the c axis. The applied field is parallel to the c axis.

where F_p is the volume pinning force, γ is determined solely by the microstructural properties of the superconductor, $B_{c2}(T)$ is the upper critical field, and $f(b) = b^p(1-b)^q$ where p and q are constants and the reduced magnetic field $b = B/B_{c2}(T)$.

There is no evidence in figures 4–6 that we have reached the phase boundary associated with the upper critical field or the irreversibility line [19]. Our high-field data are exponential up to the highest magnetic field measured at each temperature. In principle we can parameterize our data using equation (5) with most notably $B_{c2}(T)$ as a free parameter as well as n, p, and q. However, fitting our data to (5) leads to highly correlated values for the free parameters and non-physical results. Alternatively we can extrapolate $J_c(B, T)$ to zero and find a value for $B_{c2}(T)$ using a polynomial function form and part of our data set. However without any complementary information, it is probable that $B_{c2}(T)$ obtained in this way and the values for n, p, and q are artifacts of the analysis [20]. This can be contrasted to unaligned bulk polycrystalline $La_{1.85}Sr_{0.15}CuO_4$, where J_c dropped precipitously at a magnetic field similar to that found in an independent single-crystal study for the superconducting/normal phase boundary and identified as the upper critical field [21].

More recently, flux pinning models have been developed that explicitly incorporate thermally activated flux creep [22–25]. An estimate for the activation energy U_0 of the barriers restraining the flux lines has been suggested of the form [26]

$$U_0 = \mu_0 H_c^2(T)(\phi_0/B)\xi(T) \tag{6}$$

where $H_c(T)$ is the thermodynamic critical field and $\xi(T)$ is the coherence length. By including an additional logarithmic dependence of the activation energy on the applied

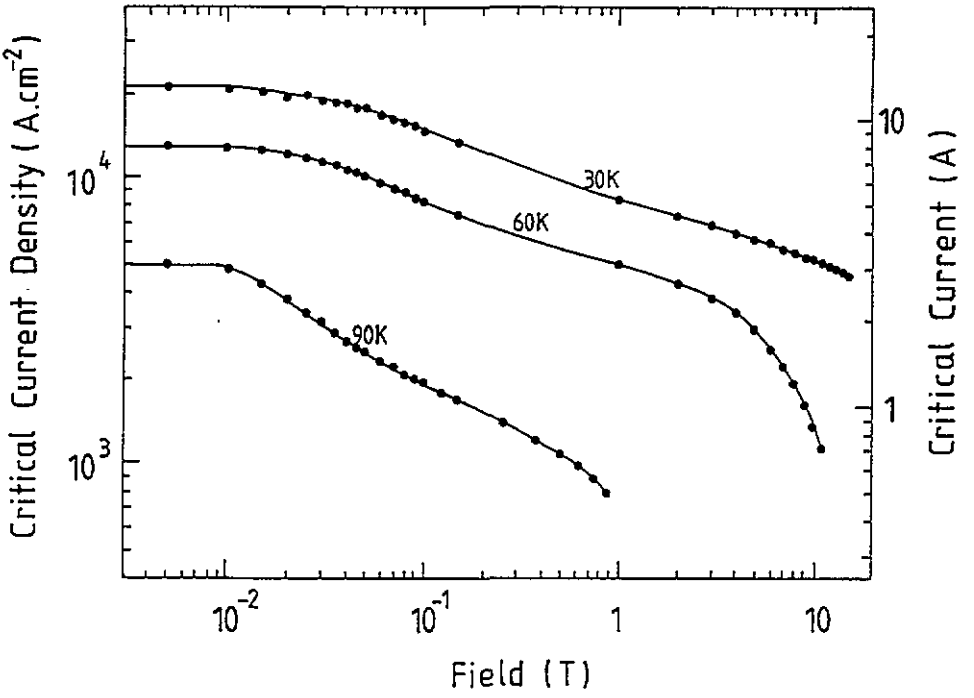

Figure 5. Log_{10} (critical current density) defined at 2 μV cm^{-1} versus the magnetic field as a function of temperature. J is orthogonal to the c axis. The applied field is orthogonal to both J and the c axis.

current [23], an expression for the critical current density, which does not obey Fietz–Webb scaling, can then be derived of the form [27]

$$J_c(B, T) = J_{c0}(T) \exp(-B \ln(E_c/E_0) k_B T/F(T)) \tag{7}$$

where $J_{c0}(T)$ is the temperature dependent depinning current in the absence of thermal fluctuations, E_c is the electric field criterion at which the critical current density is measured, $F(T)$ is a function of temperature alone and E_0 is a characteristic electric field for the material. Although equation (7) provides an exponential magnetic field dependence, a detailed microscopic theory is lacking. The factor $(\phi_0/B)\xi(T)$ in (6), which leads to the exponential field dependence in (7), is justified heuristically by assuming that the elemental movable volume in the flux line lattice has the cross-sectional area of the Abrikosov unit cell (ϕ_0/B) and length $\xi(T)$ [26]. The factor $\mu_0 H_c^2(T)$ is taken as the low-field approximation for the Gibbs free energy density $G \simeq \mu_0 H_c^2(T)(1-(H/H_{c2}(T)))^2$ [26]. Neither factor has been justified rigorously, indeed contrary to (6) resistive measurements on single crystals of $Bi_2Sr_2CaCu_2O_x$ [28] show that $U_0 \propto B^{-\eta}$ where $0.15 < \eta < 0.48$ (depending on the magnitude and orientation of the applied field). This dependence necessarily implies a term B^η in the argument of the exponential of (7), which contradicts our experimental results.

In summary, although we can in principle parameterize the data using (5) or (7), they are best described using the exponential form given by equation (4) in high magnetic fields below the irreversibility line (and $B_{c2}(T)$), which strongly suggests that a pair breaking mechanism operates.

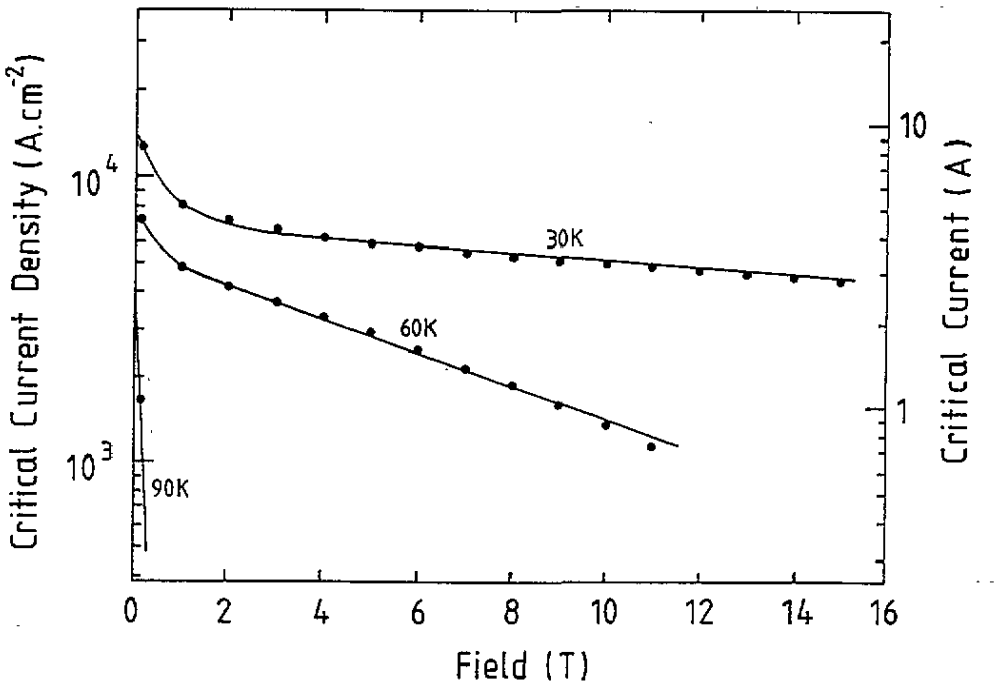

Figure 6. Log_{10} (critical current density) defined at 2 μV cm^{-1} versus the magnetic field as a function of temperature. J is orthogonal to the c axis. The applied field is parallel to J.

6. Comparison with other $J_c(B, T)$ data

6.1. Thin films

Detailed $J_c(B, T)$ data on epitaxial thin films of high-temperature superconductors have been completed by a number of groups. Because there is no normal metal in intimate contact with these films, one can measure the critical current over a very broad range. This range of measurement is not readily accessible with wires and tapes since the metal matrix, which serves as an electrical shunt, can carry a significant current at the E field used to define the critical current density. At the E field criterion of 2 μV cm^{-1} used in this work, typically 10 A cm^{-2} flows through the Ag sheath. This current in the Ag effectively produces a lower bound for the minimum critical current that can be measured. We now compare the functional form for $J_c(B, T)$ we have found in the tape that is exponential over one to two orders of magnitude to that obtained over three to five orders of magnitude in thin films.

For $Bi_2Sr_2Ca_2Cu_3O_x$ [15, 29] and $Bi_2Sr_2CaCu_2O_x$ [30] epitaxial thin films it has been found experimentally that

$$J_c(B, T) = \alpha^*(T) \exp(-\mu_0 H \cos\theta / \beta^*(T)) \tag{8}$$

where θ is the angle between the applied magnetic field and the c axis and $\alpha^*(T)$ and $\beta^*(T)$ are functions of temperature alone. $J_c(B, T)$ measurements made as a function of angle θ have shown excellent agreement with (8). Universal log–linear curves at each temperature of $J_c(B, T)$ versus $B \cos\theta$ at a fixed temperature were obtained.

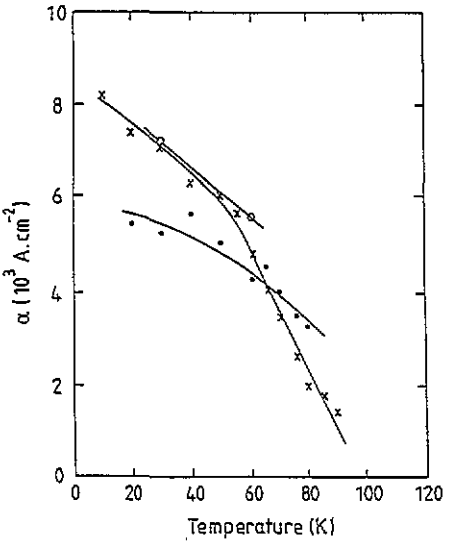

Figure 7. $\alpha(T)$ as a function of temperature: ×, J is orthogonal to the c axis, the applied field is orthogonal to both J and the c axis; ●, J is orthogonal to the c axis, the applied field is parallel to the c axis; ○, J is orthogonal to the c axis, the applied field is parallel to J.

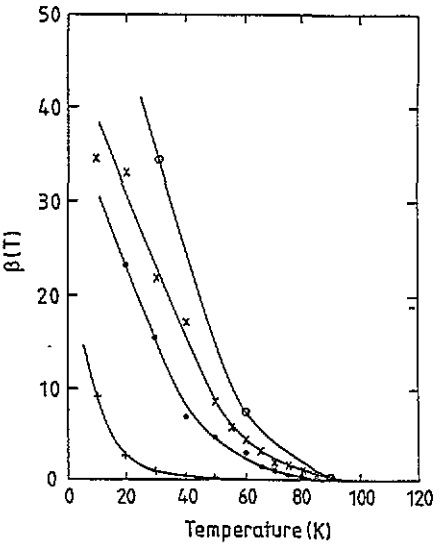

Figure 8. $\beta(T)$ as a function of temperature: ×, J is orthogonal to the c axis, the applied field is orthogonal to both J and the c axis; ●, J is orthogonal to the c axis, the applied field is parallel to the c axis; ○, J is orthogonal to the c axis, the applied field is parallel to J; +, an epitaxial thin film of $Bi_2Sr_2Ca_2Cu_3O_x$, J is orthogonal to the c axis, the applied field is parallel to the c axis [15].

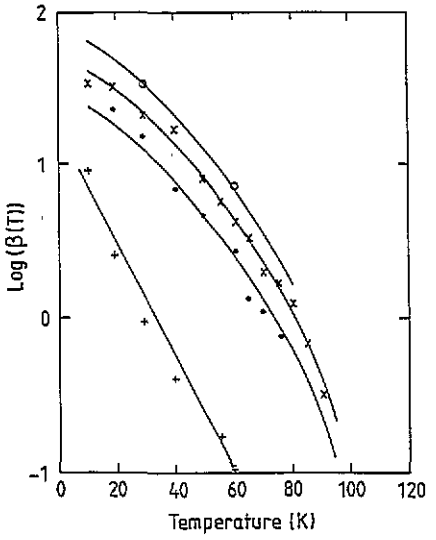

Figure 9. $\mathrm{Log}_{10}(\beta(T))$ as a function of temperature: ×, J is orthogonal to the c axis, the applied field is orthogonal to both J and the c axis; ●, J is orthogonal to the c axis, the applied field is parallel to the c axis; ○, J is orthogonal to the c axis, the applied field is parallel to J; +, an epitaxial thin film of $Bi_2Sr_2Ca_2Cu_3O_x$, J is orthogonal to the c axis, the applied field is parallel to the c axis [15].

Detailed $J_c(B, T)$ data on an epitaxial thin film of $YBa_2Cu_3O_y$ have been taken in magnetic fields up to 30 T [31]. These data show an unambiguous exponential field dependence for $J_c(B, T)$ data over five orders of magnitude in current density and hence provide evidence for a pair breaking mechanism operating at barriers in these films.

There are a number of broad similarities between the thin-film results and the $Bi_2Sr_2Ca_2Cu_3O_x$ tape.

(i) Most notably, the $Bi_2Sr_2Ca_2Cu_3O_x$, $Bi_2Sr_2CaCu_2O_x$, and $YBa_2Cu_3O_7$ thin films show an exponential field dependence for $J_c(B, T)$ in high fields as does the tape.

(ii) The functional form of $\alpha(T)$: for both the $Bi_2Sr_2Ca_2Cu_3O_x$ tape and the $YBa_2Cu_3O_7$ film, at low temperatures $\alpha(T)$ for $B \perp c$ is higher than for $B \| c$ but decreases much more rapidly as the temperature increases. This leads to a crossover in $\alpha(T)$ at about 60 K (for the Bi based films $\alpha(T)$ for $B \perp c$ is equal to that for $B \| c$ throughout the temperature range in agreement with equation (8)).

(iii) The functional form of $\beta(T)$: for the $Bi_2Sr_2Ca_2Cu_3O_x$, $Bi_2Sr_2CaCu_2O_x$, and $YBa_2Cu_3O_7$ thin films and the tape the temperature dependence of $\beta(T)$ is convex; the temperature dependence of $\beta(T)$ for the $Bi_2Sr_2Ca_2Cu_3O_x$ and the $Bi_2Sr_2CaCu_2O_x$ thin films and the tape is independent of the orientation of the magnetic field.

6.2. Tapes

We can consider whether the difference between the functional form of $J_c(B, T)$ for the Bi based epitaxial thin films and the tape is solely due to the imperfect texturing of our tapes. Within the framework of (8), such a simple description implies that $\alpha(\phi, T)$ must be independent of orientation of magnetic field. The variable-temperature data shown in figure 7 demonstrate that unlike the thin-film case, $\alpha(\phi, T)$ depends on the orientation of the magnetic field hence imperfect texturing alone cannot explain our results. Other authors have found that measurements on $Bi_2Sr_2Ca_2Cu_3O_x$ tapes at liquid nitrogen (LN) temperatures were consistent with (4) [6]. We suggest that this may have occurred because of the crossover of $\alpha(\phi, T)$ at LN temperatures and is not generally valid at all temperatures.

If we make the most simple assumption, namely that the distribution in misalignment can be described by a single characteristic angle, we can compare the magnetic field dependence of the $J_c(B, T)$ in the tape with the thin-film results using (4) and (8) by equating $\cos\theta$ to $f(\theta)$, $\beta^*(T)$ to $\beta^{\#}(T)$, and $\alpha(\phi, T)$ to $\alpha^*(T)$. If we assume that the location of the percolative current path does not change when B is rotated, from the results given in (3), the calculated characteristic misalignment angles are 20° and 31° parallel and orthogonal to the direction of rolling respectively. A description of the current path through these tapes is a very complex percolation problem. Nevertheless these angles seem rather large given that the mosaic spread in the grains themselves is expected to be about 12° [6, 32]. In addition, the temperature dependences of $\beta(T)$ shown in figure 9 are markedly different in the $Bi_2Sr_2Ca_2Cu_3O_x$ thin film and in our tape.

We conclude that neither imperfect texturing nor a percolative path of well connected (quasisingle-crystalline) material can alone explain the differences between our tape and the thin film.

7. Discussion

Optimizing the fabrication of bulk polycrystalline high-temperature superconductors to carry high critical currents in high magnetic fields dramatically changes the functional form of the field and temperature dependence of $J_c(B, T)$.

Poorly optimized samples show Josephson junction [33] or weak-link behaviour [34, 35] such that very weak magnetic fields reduce the critical current to zero. These properties, which occur when the grain boundaries are not transparent to the superelectrons on the scale of the coherence length, have been addressed in detail in the literature [36].

High-temperature superconductors have spawned a wide variety of experimental functional forms and theoretical models for $J_c(B, T)$. The flux pinning models used to describe $J_c(B, T)$ in low-temperature superconductors [37, 38] have been developed to include the intrinsic anisotropy [39–41] and the short coherence length as well as the high critical temperature, and hence possible thermally activated processes [42], of the high-temperature superconductors [43, 44].

Despite the range of theoretical models and experimental data in the literature, in this work we provide some experimental evidence for similarities in $J_c(B, T)$ for an optimized tape and epitaxial thin films of high-temperature superconductor.

We suggest that in the tape there are regions of strong pinning separated by barriers. We can contrast a superconductor in which pair breaking limits $J_c(B, T)$ to that in which a flux pinning mechanism operates. In the former case, the supercurrent must cross extended barriers in which the superconductivity is depressed. When the magnetic field is increased, the number of electrons in the barrier is decreased, which in turn decreases $J_c(B, T)$. In the latter case, the crucial feature is the presence of localized pinning sites that restrain the fluxons. The critical current density is determined by the forces on the fluxons and the density of superelectrons is of secondary importance.

7.1. The barriers

The grain boundaries are the most obvious microstructural feature in the $Bi_2Sr_2Ca_2Cu_3O_x$ tape that could act as a tunnelling barrier to superelectrons. AC magnetization measurements [45], which measure the flux profile across the sample and provide an estimate of the local variation of the critical current density, have been completed on similar tapes to those presented here. These magnetic results suggest that the tapes are granular such that the magnitude of the intragranular J_c is two or three orders of magnitude higher than the intergranular (transport) J_c. Measurements of the DC magnetic properties of $Bi_2Sr_2Ca_2Cu_3O_x$ powders and tapes (before and after fracturing) demonstrate that the transport current density is determined by the properties at the grain boundaries [46]. Whether current flow from grain to grain is primarily along the c axis [47] or between slightly misoriented Cu–O planes across low-angle grain boundaries is not yet clear [6]. Neither description is inconsistent with a pair breaking mechanism operating at barriers.

Although there are broad similarities between the magnetic field, temperature, and configuration dependences of $\alpha(\phi, T)$ and $\beta(\phi, T)$ in the epitaxial thin films and the tape, nevertheless the precise temperature dependence of $\alpha(\phi, T)$ and $\beta(\phi, T)$ are not the same. This implies that the nature of the pair breaking mechanism at the barriers in these different materials is not identical. Twin boundaries and low-angle grain boundaries are obvious candidates as barriers in the epitaxial thin films. Nevertheless, we leave open the question of the location of the barriers in these films.

The phenomenological pair breaking S–N–S model that describes the exponential field dependence of our high-field $J_c(B, T)$ data cannot explain the temperature dependence of $\beta(\phi, T)$ either in our tapes or in epitaxial Bi based thin films. Measurements on S–N–S junctions using low-temperature superconductors confirm that $\beta(T)$ is temperature independent in agreement with (2) [48]. However as the temperature increases, the electron scattering length in a clean normal barrier should decrease and hence $\beta(T)$ should increase. Experimentally in the thin films and our tape, $\beta(\phi, T)$ decreases as temperature increases and hence is inconsistent with the detailed predictions of the phenomenological S–N–S model for normal metals in the clean limit. It has been suggested that the crystallographic disorder and the electron scattering at the grain boundaries in superconductors may result in a normal

layer [49]. However at present we have no adequate mathematical description of such grain boundaries that can be incorporated in De Gennes' very general formalism.

Some theoretical work on flux pinning [24, 25] and pair breaking [50] (Josephson tunnelling) mechanisms has shown an exponential field dependence for $J_c(B, T)$ in some limiting cases. At present it is unclear whether this work can be developed to describe the large range of magnetic field over which we have found an exponential dependence for $J_c(B, T)$ or provide a clear explanation for the temperature dependence we have found for $\alpha(T)$ and $\beta(T)$. Electromagnetic measurements of the type that Dimos *et al* [51] initiated on bicrystals of $YBa_2Cu_3O_y$ may help us to locate the pair breaking. Clearly a better understanding of the structure and electromagnetic properties of grain boundaries will be required to proceed further.

8. Concluding comments

We have measured the critical current of an optimized bulk aligned $Bi_2Sr_2Ca_2Cu_3O_x$ tape in three configurations of transport current, magnetic field, and the superconducting tape from 10 K up to T_c in magnetic fields up to 15 T. In all three configurations, we find the critical current density can be described by

$$J_c(B, T) = \alpha(\phi, T) \exp[-\mu_0 H/\beta(\phi, T)]$$

where $\beta(\phi, T)$ is of a separable variable form $\beta(\phi, T) = \beta^{\#}(T)/f(\phi)$, $\beta^{\#}(T)$ is a function of temperature alone, and $f(\phi)$ is a constant dependent only on the orientation of B, J, and the c axis.

A similar but not identical exponential magnetic field dependence has been found in $Bi_2Sr_2Ca_2Cu_3O_x$, $Bi_2Sr_2CaCu_2O_x$ and $YBa_2Cu_3O_y$ thin films. This exponential magnetic field dependence provides evidence that a pair breaking mechanism operates at barriers in these materials. We have concluded that pair breaking operating at the grain boundaries determines $J_c(B, T)$ in the $Bi_2Sr_2Ca_2Cu_3O_x$ textured tape.

Acknowledgments

We acknowledge the help of Mrs P Russell in the production of the figures. The work was supported by the EPSRC.

References

[1] Heine K, Tenbrink J and Thoner M 1989 *Appl. Phys. Lett.* **55** 2441
[2] Sato K, Hikata T, Mukai H, Ueyama M, Shibuta N, Kato T, Masuda T, Nagata M, Iwata K and Mitsui T 1991 *IEEE Trans. Magn.* **MAG-27** 1231
[3] Kato T, Hikata T, Uemeya M, Sato K and Iwasa Y 1992 *MRS Bull.* **52** and companion articles therein
[4] Haldar P, Hoehn J G, Rice J A, Motowidlo L R, Balachandran U, Youngdahl C A, Tkaczyk J E and Bednarczyk P J 1993 *IEEE Trans. Appl. Supercond.* **AS-3** 1127
[5] Takahashi C, Komatsu M, Yaegashi Y, Nagano M, Takahashi H, Hamada K and Nagata A 1993 *IEEE Trans. Appl. Supercond.* **AS-3** 957
[6] Hensel B, Grivel J C, Jeremie A, Perin A, Pollini A and Flukiger R 1993 *Physica* C **205** 329
[7] Tkacyz J E, Arendt R H, Garbauskas M F, Hart H R, Lay K W and Luborsky F E 1992 *Phys. Rev.* B **45** 12506

[8] Maley M P, Kung P J, Coulter J Y, Carter W L, Riley G N and McHenry M E 1992 *Phys. Rev.* B **45** 7566
[9] Feng Y, Hautanen K E, High Y E, Larbalestier D C, Ray R, Hellstrom E E and Babcock S E 1992 *Physica* C **192** 293
[10] Osamura K, Ochiai S and Murayama T 1993 *Proc. 5th Int. Symp. on Superconductivity ISS 1992 (Tsukuba)* ed Y Bando and H Yamauchi (Berlin: Springer) p 689
[11] Hampshire D P and Jones H 1987 *J. Phys. E: Sci. Instrum.* **20** 516
[12] Friend C M and Hampshire D P 1994 *J. Meas. Sci. Technol.* accepted for publication
[13] De Gennes P G 1964 *Rev. Mod. Phys.* **36** 225; 1966 *Superconductivity of Metals and Alloys* (New York: Benjamin)
[14] Hsiang T Y and Finnemore D K 1980 *Phys. Rev.* B **22** 154
[15] Yamasaki H, Endo K, Kosaka S, Umeda M, Misawa S, Yoshida S and Kajimura K 1993 *IEEE Trans. Appl. Supercond.* **AS-3** 1536
[16] Hampshire D P, Clark A F and Jones H 1989 *J. Appl. Phys.* **66** 3160
[17] Hampshire D P, Jones H and Mitchell E W J 1984 *IEEE Trans. Magn.* **MAG-21** 289
[18] Fietz W A and Webb W 1969 *Phys. Rev.* **178** 657
[19] Huse D A, Fisher M P A and Fisher D S 1992 *Nature* **358** 553
[20] Hampshire D P 1993 *Eur. Conf. on Applied Superconductivity (Göttingen)* ed H C Freghardt (Informationsgesellschaft Verlag) p 873
[21] Hampshire D P, Ikeda J A S and Chiang Y M 1989 *Phys. Rev.* B **40** 8818
[22] Yeshurun Y and Malozemoff A P 1988 *Phys. Rev. Lett.* **60** 2202
[23] Zeldov E, Amer N M, Koren G and Gupta A 1990 *Appl. Phys. Rev.* **56** 1700
[24] Vinokur V M, Feigelman M V and Geshkebein V B 1991 *Phys. Rev. Lett.* **67** 915
[25] Feigelman M V, Geshkebein V B, Larkin A I and Vinokur V M 1989 *Phys. Rev. Lett.* **63** 2303
[26] Tinkham M 1988 *Phys. Rev. Lett.* **61** 1658
[27] Neumeller H W, Gerhauser W, Ries G, Kummeth P, Schmidt W, Klaumunzer S and Saemann-Ischenko G 1993 *Cryogenics* **33** 14
[28] Palstra T M, Batlogg B, Schneemeyer L F and Waszczak J V 1988 *Phys. Rev. Lett.* **61** 1662
[29] Endo H, Yamasaki H, Misawa S, Yoshida S and Kajimura K 1992 *Nature* **355** 327
[30] Schmitt P, Kummeth P, Schultz L and Saemann-Ischenko G 1991 *Phys. Rev. Lett.* **67** 267
[31] Hampshire D P and Chan S-W 1992 *J. Appl. Phys.* **72** 4220
[32] Willis J O, Coulter J Y, Salazar K V, Peterson E J, Daeman L and Bulaevskii L N 1993 *ICMC 93 (Albuquerque, 1993)*
[33] Josephson B D 1962 *Phys. Lett.* **1** 251
[34] Bardeen J, Ginsberg D M and Salamon M B 1987 *Proc. Int. Workshop on Novel Mechanisms of Superconductivity (Berkeley, CA, 1987)* ed S A Wolf and V Z Kresin (New York: Plenum) p 7
[35] Deutscher G and Muller K A 1987 *Phys. Rev. Lett.* **59** 1745
[36] Peterson R L and Ekin J 1988 *Phys. Rev.* B **37** 9848
[37] Brandt E H 1977 *J. Low Temp. Phys.* **26** 709
[38] Dew-Hughes D 1974 *Phil. Mag.* **30** 293
[39] Tachiki M and Takahashi S 1989 *Solid State Commun.* **72** 1083
[40] Kes P M, Aarts J, van der Berg I, van der Beek C L and Mydosh J A 1989 *Supercond. Sci. Technol.* **1** 242
[41] Clem J R 1991 *Phys. Rev.* B **43** 7837
[42] Malozemoff A P 1991 *Physica* C **185–189** 264
[43] Brandt E H 1991 *J. Mod. Phys.* B **5** 751
[44] Feigelman M V and Vinokur V M 1990 *Phys. Rev.* B **41** 8986
[45] Hautanen K E, Oussena M and Cave J R 1993 *Cryogenics* **33** 327
[46] Knaak W 1992 *Supercond. Sci. Technol.* **5** 134
[47] Bulaevskii L N, Clem J R, Glazman L I and Malozemoff A P 1992 *Phys. Rev.* B **45** 2545
[48] Finnemore D K, Ostenson J E, Ji L, McCallum R W and Clem J R 1988 *Adv. Cryo. Eng.* **35** 613
[49] Dew-Hughes D 1982 *Mater. Lett.* **1** 41
[50] Bulaevskii L N, Daemen L, Maley M P and Coulter J Y *Los Alamos Internal Report* LA-UR-93-409
[51] Dimos D, Chaudhari P and Mannhart J 1990 *Phys. Rev.* B **41** 4038